Journal of Physics and Chemistry of Solids 81 (2015) 57–65

Contents lists available at ScienceDirect

Journal of Physics and Chemistry of Solids

journal homepage: www.elsevier.com/locate/jpcs

Synthetic hydroxyapatites doped with Zn(II) studied by X-ray diffraction, infrared, Raman and thermal analysis

José R. Guerra-López [a,*], Gustavo A. Echeverría [b,c], Jorge A. Güida [a,c,d], Raúl Viña [b], Graciela Punte [b]

[a] Departamento de Básicas, Universidad Nacional de Luján, ruta 5 y 7, CC, 6700 Luján, Argentina
[b] LANADI e IFLP (CCT-La Plata), Departamento de Física, Facultad de Ciencias Exactas, Universidad Nacional de La Plata, CC67, 1900 La Plata, Argentina
[c] Departamento de Ciencias Básicas Facultad de Ingeniería, Universidad Nacional de La Plata, 115 y 49, 1900 La Plata, Argentina
[d] CEQUINOR (CCT-La Plata), Facultad de Ciencias Exactas, Universidad Nacional de La Plata, CC 962, 1900 La Plata, Argentina

ARTICLE INFO

Article history:
Received 22 September 2014
Received in revised form
26 January 2015
Accepted 30 January 2015
Available online 7 February 2015

Keywords:
Hydroxyapatite cationic substitution
Infrared and Raman spectroscopis
Second derivative spectra
Rietveld analysis
Thermal treatment

ABSTRACT

Calcium hydroxyapatite (CaHap) formation when different amounts of Zn(II) are present in the mother solution has been investigated by atomic absorption, infrared and Raman spectroscopies, X-ray diffraction and thermal analysis (DTA and TG). The studied samples have been synthesized at $T=95$ °C and pH 9 in air. The analysis of the results have shown that the pure CaHap sample crystallizes in the monoclinic form $P2_1/b$. Concentrations up to 20% of Zn(II) in the mother solution, equivalent to smaller concentrations in solid (up to 9.1% in wt), favor the formation of the hexagonal apatite, $P6_3/m$, while Zn(II) concentrations higher than 20% in solution help an amorphous phase development where vibrational spectra indicated coexistence of two phases: an apatite and $ZnNH_4PO_4 \cdot H_2O$. Infrared data of thermal treated samples endorse that HPO_4^{2-} ion had not been incorporated in Zn(II) doped samples during the synthesis process. Present results also allow to conclude that Zn(II) cation exhibits a preference to occupy the Ca2 site of the apatite structure and induces water adsorption and a small quantity of CO_3^{2-} cation incorporation, leading to formation of a less crystalline Ca deficient apatite.

1. Introduction

Calcium hydroxyapatite, $Ca_{10}(PO_4)_6(OH)_2$ (CaHap), plays a very important role on earth. From the biological point of view, it is the major constituent of the skeleton and teeth of vertebrates. It is important as a catalysis carrier, in the fertilizer industry and in chromatography [1–3]. It easily forms solid solutions via chemical reactions with various metal oxides, halides, and carbonates. Apatite can incorporate several substituents, while keeping its basic structure. Ca(II) can be substituted, to some extent, for monovalent (Na(I), K(I)) [4], divalent (Sr(II), Ba(II), Pb(II)) [5–7] and trivalent (Y(III)) cations [4,8]. Among the anionic substitutions, the significant ones are: replacement of OH^- by CO_3^{2-} [3,9,10], F^- [10–12] and Cl^- [11], and PO_4^{3-} by CO_3^{2-}, HPO_4^{2-} [9,13], AsO_4^{3-} and VO_4^{3-} [14]. Some substitutions are coupled with others [1,9,15,16] to maintain charge balance in the apatite phase, e.g. CO_3^{2-} for PO_4^{3-} is coupled with Na(I) by Ca(II). The trivalent anionic phosphate sites cannot accept vacancies, probably because they are quite large and vacancies would destabilize the lattice [9,17]. On the contrary the cationic sites can accept vacancies; up to a maximum of two sites out of the ten available in stoichiometric apatites [9,13,17].

Due to its interesting chemical and physical properties, synthetic CaHap finds various applications, not only as a biomaterial, but also as adsorbent in chromatography, to separate proteins and enzymes [18]; as a catalyst, for dehydrogenation and dehydration of alcohols [19], and as an effective means for water contaminants removal [20].

To increase the natural biocompatibility and improve the biofunctionality of CaHap, its capacity to host different chemical species has been explored. The most common example is the preparation of carbonate-substituted [1,9,17] and fluoride-substituted CaHap [4,21]. Another potential method for improving the biological activity of CaHap is the incorporation of divalent cations (Mg, Sr, Zn or Ba) into its lattice [4,8,22,23]. Among the cations known as substituents in the CaHap lattice, Zn(II) deserves some attention because it is one of the essential trace elements in human bone and plasma [24–29]. The important role of zinc in many biological functions is well known: zinc inhibits, in the concentration range of 10^{-8}–10^{-5} M (0.65 μg $L^{-1}$to 0.65 mg L^{-1}), osteoclast-like cell formation in mouse marrow cell cultures and, in concentrations as low as 10^{-14} M (0.65 pg L^{-1}), constraints rats

* Corresponding autor.
E-mail address: jguerra@coopenetlujan.com.ar (J.R. Guerra-López).

http://dx.doi.org/10.1016/j.jpcs.2015.01.017
0022-3697/

osteoclastic bone resorption in vitro [30,31]. Moreover, zinc deficiency causes bone growth retardation [32,33]. However, reports on its applications in dentistry are contradictory. Several clinical studies have demonstrated that zinc salts, alone or in combination with antimicrobial agents (e.g triclosan or chlorhexidine) were effective in reducing calculus formation [32,33]. But, Jenking et al. have reported the opposite [34]. Furthermore, according to the literature, its presence is expected to inhibit apatite formation favoring instead the development of other phosphates [3,11,35]. Therefore, possible Zn incorporation into the biological fluids due to its elution from dental casting and prosthesis alloys requires further investigation.

In present work phosphates of Ca and Ca/Zn, were prepared from aqueous solutions in conditions of reaction different from those ones found in the literature [36,37]. The aim of the investigation is to get a better understanding of the influence of Zn on biological systems and mineralization processes and to add to the development of calcium phosphate biomaterials incorporating optimum levels of zinc to mimic bone. The relationship between the proportion of Zn (II) cation present in the mother solution and the structural properties of the solid products of the reaction were studied by complementary techniques, X-ray powder diffraction (XRPD) data Rietveld analysis, thermogravimetry and Raman and IR spectroscopies, the later including second derivative analysis and the examination of samples treated at different temperatures. The results and their potential biological implications are discussed below.

2. Experimental

2.1. Synthesis and processing

Analytical reagent grade chemicals and freshly distilled water were used throughout the preparation of the solutions. The Hakey and Newesely method [38], with small modifications [13], was employed to synthesize the samples used to study the effect of the presence of Zn (II) in the formation of calcium phosphates. Over a stirred solution of ammonium acetate two solutions 0.2 M (one of calcium and zinc acetate and other of ammonium phosphate) were added dropwise. The solution composition in each synthesis was attained by modification of the relative content of calcium and zinc. The initial solution had a 100% of calcium and it was progressively changed up to reach a solution composition of 25% of zinc and 75% of calcium acetate. During crystallization the temperature of the solution was kept at 95 °C and the pH at 9. The precipitates were left 30 h in their mother solution and afterward they were filtered, washed with distilled water and dried at 100 °C. The amount of H_3O^+ in solution changes during the synthesis. Therefore, to maintain the pH of the solutions constant, either NH_3 or 0.1 M acetic acid was added; pH was controlled by means of a MV 870 digital pH meter and a combined glass electrode. The electrode was calibrated at 25 °C with a buffer prepared according to the National Bureau of Standards [39].

The samples were named according to their zinc proportion in the mother solution composition (Zn/(Ca+Zn) × 100): CaHap, (Ca, Zn)Hap: Zn3, Zn5, Zn10, Zn15, Zn20 and Zn25.

2.2. Characterization

The powder samples were characterized by Chemical analysis, IR and Raman spectroscopies, XRPD, DTA and TG. The Ca and Zn content of the solid products were determined by atomic absorption spectrometry (Perkin-Elmer Model 3110) and phosphorus was determined spectrophotometrically by a method developed by Portal [40]. For IR absorption analysis, 1 mg of the powdered sample was carefully mixed with 300 mg of KBr (infrared grade) and pelletized under vacuum. The FTIR spectra at room temperature were recorded with a Bruker 66 spectrometer in the range 4000–400 cm^{-1}. The Raman spectra (at room temperature) of these compounds were recorded using a Bruker IFS-66 (3500–100 cm^{-1}) instrument provided with a Raman FRA-106 accessory and Nd: YAG laser (NIR range, 1064 nm). The second derivative of infrared spectra (in absorbance) has been performed for all synthesized samples. The derivative algorithms were performed with the Opus (Bruker) software based on the Stavitzky and Golay method [13]. The absorption data (converted from transmittance spectra) was treated with a 9 point S-G smooth. The X-ray diffraction data were obtained with a Philips PW1710 powder diffractometer with a scintillation counter and an exit beam graphite monochromator using CuKα radiation ($\lambda = 1.5406$ Å). The 2 θ range covered was from 7° to 120° with a step interval of 0.02° and a counting time of 5 s. The Rietveld analysis of the XRPD patterns from samples CaHap and Zn10, collected with a counting time of 12 s, was done as implemented in the Fullprof code [41]. Thermogravimetric (TG) and differential thermal analysis (DTA) measurements were performed with a Shimadzu system (models TGA-50 and DTA-50), working under a constant N_2 flow (50 mL min^{-1}), at a heating rate of 10 °C min^{-1}, in the temperature range: 25–1000 °C. Al_2O_3 was used as a DTA standard. Sample quantities ranged between 10 and 15 mg.

3. Results

3.1. Atomic absorption

The results of the chemical analysis of the synthesized (Ca, Zn) Hap samples are collected in Table 1. The molar Ca+Zn/P ratio found in the solid was in the range of 1.46–1.67. According to molar ratio, there was good agreement between the analytical determination and stoichiometric values of zinc for Zn3 and Zn5 samples, while samples with higher Zn content in the mother solution showed less Zn incorporation in final reaction products than the reactant composition suggested. It should be noted that atomic absorption measurements showed that the variation of the Zn concentration in the solid phase and in solution follow a linear behavior from Zn3 (99%) to Zn20 (70%). However, in Zn25 sample the Zn concentration in the solid phase increases about 3.6% (out of linearity). This behavior could be attributed to the coexistence of phases (see spectroscopic and diffraction results below).

Table 1
Inclusion of Zn(II) in solid phase.

Initial Zn(II) in preparation		Synthesis results			
X=Zn (% in mol)[a]	Zn (in wt)	Zn in solid (wt)[b]	% Zn in solid (wt)	% Zn in solution (wt)	Molar ratio (Ca+Zn)/P
3	2.0	1.9 ± 0.1	99.0	1.0	1.67
5	3.2	3.0 ± 0.1	94.0	6.0	1.67
10	6.5	5.0 ± 0.1	77.0	23.0	1.58
15	9.3	7.0 ± 0.1	75.0	25.0	1.53
20	13.0	9.1 ± 0.1	70.0	30.0	1.46
25	16.3	12.0 ± 0.1	73.6	26.4	N.D.[c]

[a] Initial zinc concentration before reaction, calculated from: Zn/(Ca+Zn) × 100; x is related to apatite formula: $Ca_{(10-x)}Zn_x(PO_4)_6(OH)_2$.
[b] Zinc concentration was quantified by Atomic absorption (AA).
[c] N.D.: Not determined because mixed phases might have been formed (see vibrational spectra discussion).

Table 2
Observed Raman wavenumbers (cm^{-1}) for CaHap and (Ca, Zn)Hap.

Mode[a]	CaHap	Zn5	Zn15	Zn20
ν_3 (E_{1u})	1103	N. D.[b]	N. D.	N. D.
ν_{3a} (E_{2g})	1072	N. D.	N. D.	N. D.
ν_{3b} (A_g)	1045	1048	1048	1048
ν_{3c} (E_{1g})	1038	N. D.	N. D.	N. D.
ν_{3b} (E_{2g})	1025	N. D.	N. D.	N. D.
$\nu_1(A_g+E_{2g})$[c]	961	963	963	963
ν_{4a} (E_{2g})	612	N. D.	N. D.	N. D.
ν_{4a} (A_g)	605	N. D.	N. D.	N. D.
ν_{4b} (E_{2g})	589	592	592	592
ν_{4c} (E_{1g})	578	581	581	581
ν_{2a} (E_{2g})	445	N. D.	N.D.	N. D.
ν_{2b} (E_{1g})	430	430	432	432

[a] J. C. Elliot. In: Elsevier SCIENCE B. V. (ed) Amsterdam, Structure and Chemistry of the Apatites and Other Calcium Orthophosphates. Amsterdam, The Netherlands, 1994, pp 103.
[b] N. D.: Not detected
[c] The plus sign does not mean combination modes.

3.2. Vibrational spectra

The solids were analyzed by Raman and infrared spectroscopies to obtain information about possible local distortions induced by Zn in the apatitic structure. All the internal Raman and IR-active vibrations of the phosphate ions in the apatite phase are listed in Tables 2 and 3, respectively.

3.2.1. Raman spectra

3.2.1.1. Stoichiometric hydroxyapatite. Fig. 1 shows the Raman spectra of synthesized solids in different Zn proportion for selected spectral region, including pure apatite spectrum for comparison. Stretching and librational modes of hydroxyl ions were not observed in these spectra, in spite these bands (although weak) had been reported previously [9,42]. Therefore, attention was focused on the phosphate modes.

Some of the characteristic wavenumbers for phosphate anion in hydroxyapatite are compiled in Table 2, where the four internal vibrational modes are included. The most intense bands at 961 cm^{-1} have been assigned to the symmetric $\nu_1(PO_4)$ A_1 stretching mode of the 'free' tetrahedral phosphate ion. Contrary to data reported by Nelson and Williamson [42], no splitting of this band has been observed. Apart from the $\nu_1(PO_4)$, two $\nu_2(PO_4)$ bands, five $\nu_3(PO_4)$ bands and four $\nu_4(PO_4)$ bands were resolved. No other additional bands were observed after a careful analysis of the spectra. This finding would allow to discard the presence of any impurity such as HPO_4^{2-} in the solid phase.

3.2.1.2. Zinc–CalciumHap. Fig. 1 allows to compare the Raman spectrum of pure CaHap with spectra coming from CaHap doped with different amounts of Zn(II). Corresponding band positions are collected in Table 2. A small shift from 961 to 963 cm^{-1} is observed for the $\nu_1(PO_4)$ band when zinc is first incorporated into the structure, sample Zn5. No further shift could be detected with

Table 3
FT-IR spectra phosphate bands assignments in CaHap.

Mode	CaHap	Zn5	Zn15	Zn20
ν_{3a} (A_g)	1090	1096	1096	1096
$\nu_{3b}+\nu_{3b}$ ($E_{1u}+A_u$)[a]	1050	1035	1035	1035
ν_1 (E_{1u})	961	963	963	963
ν_{4a} (E_{1u})	602	604	604	604
$\nu_{4b}+\nu_{4c}$ (A_g+E_{1u})[a]	571	565	565	565
ν_{2a} (A_u)	473	476	476	476

[a] The plus sign does not mean combination modes.

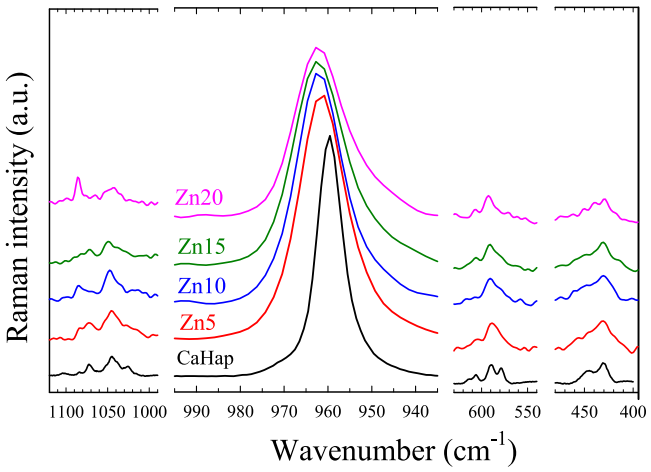

Fig. 1. Raman spectra of CaHap and Zn(II) dopped CaHap in the range 1100–400 cm^{-1}.

increase of Zn content in the solid phase. The P–O antisymmetric stretching of phosphate ions, ν_3, appears in the region 1020–1100 cm^{-1}. Due to the weakness of the signal this mode offers small information in the Raman spectra.

Only a little shift to higher wave number is observed for the most intense band at 1045 cm^{-1} (ν_{3b} A_g) (for comparison with CaHap see Table 2). The remaining phosphate modes were observed in the region of lower frequencies, (600–400 cm^{-1}) corresponding to bending modes ν_2 and ν_4. Most intense band for both modes shift to higher wavenumber for any sample doped with Zn, as found in the stretching modes. The fine structure observed for CaHap modes blurs for any sample containing Zn, but not progressive effect with Zn concentration increase is detected.

Bands corresponding to C–O vibrations: ν_1 (strong) at about 1080 cm^{-1}, ν_3 (weak) between 1410 and 1470 cm^{-1} and ν_2 between 850 and 890 cm^{-1}, characteristic of the carbonate group, are neither observed in the FT-Raman spectrum of CaHap nor in the spectra of (Ca, Zn)Hap as prepared samples. Therefore, from these data, there is no evidence for the presence of carbonate or other impurities in any of the as prepared samples.

3.2.2. Infrared spectra

The powder infrared spectrum of the CaHap is presented in Fig. 2. It is characterized by the following absorption modes: OH^- stretching (ν(OH)=3572 cm^{-1}) and librational (L(OH)=630 cm^{-1}),

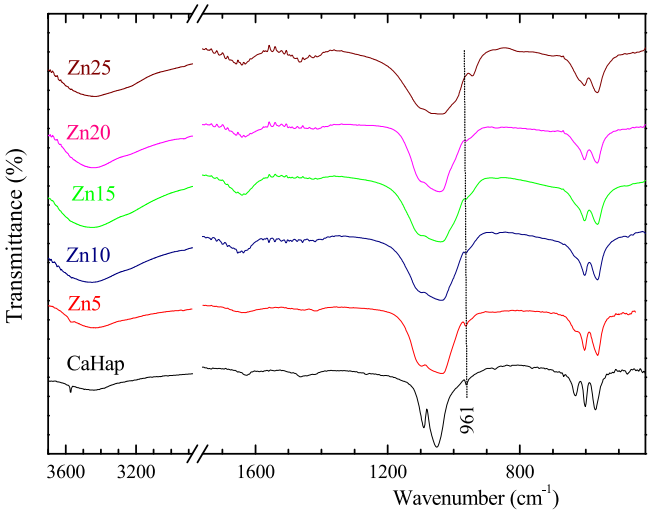

Fig. 2. Infrared spectra of CaHap and Zn(II) dopped CaHap.

and PO_4^{3-} (ν_3 1090 and 1050 cm^{-1}, ν_1 961 cm^{-1}, ν_4 602 and 571 cm^{-1}, ν_2 473 cm^{-1}). The broad and weak bands at 3452 and 1631 cm^{-1} in CaHap are due to the presence of water in the solid (mainly adsorbed water) [10,13,22,29,43], see additional discussion in thermal analysis section. The broad band from about 3700 cm^{-1} to 3000 cm^{-1} corresponds to the overlapping of ν_3 and ν_1 stretching modes, widened by hydrogen-bond formation. Band at 1630 cm^{-1} has been assigned to the ν_2 bending mode of the H_2O molecules.

The substitution of Ca(II) for Zn(II) in apatite leads to changes in the infrared spectra. As the zinc concentration increases the intensity of water bands (3452 and 1631 cm^{-1}) rises. This behavior is shown in Fig. 2. Concerning the OH^- group vibrations, the stretching band suffers a small shift to lower wavenumbers (3569 cm^{-1} for Zn5 sample) and a strong reduction of its intensity when Zn is incorporated in the apatite structure. An opposite behavior is observed for the corresponding librational mode which shifts towards higher wavenumbers (633 cm^{-1} for the same sample). The intensity of the bands corresponding to OH^- modes of CaHap decreases in the presence of increasing concentrations of zinc, as mentioned before. The absorption bands assigned to PO_4^{3-} in CaHap, see Table 3, are present in all spectra up to Zn20. Small shifts are observed for most of the modes when going from CaHap to Zn5, but no appreciable additional shifts are observed in (Ca, Zn)Hap as prepared samples with higher Zn concentration.

Bands broadening in the region 1100–1000 (ν_3) and at around 565 (ν_4) were also observed in the (Ca,Zn)Hap samples. The intensity of bands at 476 and 963 cm^{-1} progressively decreases with the increase of zinc concentration in solid; for the concentration of 9% (sample Zn20) they are almost absent.

The appearance of a band at 941 (ν_1) cm^{-1} and a shoulder at 619 (ν_4) cm^{-1} in the Zn25 spectrum evidenced that the increase of Zn(II) concentration in solution generates a second phase in the solid state of the as prepared Zn25 sample. This second phase might correspond to $ZnNH_4PO_4 \cdot H_2O$, which could have crystallized during the synthesis process. An additional weak band at about 1430 cm^{-1} was assigned to $\delta(NH_4^+)$, further supporting the existence of the $ZnNH_4PO_4 \cdot H_2O$ phase in this sample.

Very weak bands have been detected between 1410 and 1470 cm^{-1}, they would indicate a small amount of CO_3^{2-} in all samples, possible due to atmospheric CO_2 absorption during the synthesis. The intensity of these bands (the most intense CO_3^{2-} mode (ν_3) in IR spectra) does not increase with Zn incorporation. As expected, weaker bands of CO_3^{2-}, corresponding to ν_4 and ν_1 modes, were not observed. The small signal at about 872 cm^{-1} might be due to the $\nu_2(CO_3)$ mode, whose intensity is about one fifth of that of $\nu_3(CO_3)$. However, it might also come from the HPO_4^{2-} band at 875 cm^{-1} if these anions were present. It should be noted that other absorption bands, characteristic of the hydrogen phosphate (HPO_4^{2-}) ion, were not seen at 1100 and 530 cm^{-1}. The possible presence of HPO_4^{2-} ion will be further analyzed below in Thermal Behavior (see Section 3.4).

3.2.3. Infrared second derivative spectra

Derivative spectra are of considerable potential value because of their inherent capability to discriminate overlapped peaks. Second derivative line shape is intrinsically narrower than that of the absorption one enhancing spectral resolution [11,13,17] Therefore, second derivative spectra of all as prepared samples were performed in order to improve the analysis of the spectral changes occurring as a consequence of the incorporation of zinc in the solid phase. Particular attention has been paid to regions 500–700 cm^{-1} (ν_4 (PO_4) and ν_{lib}(OH) domains) and 900–1200 cm^{-1} (ν_1 and ν_3 PO_4^{3-} stretching modes) (Fig. 3).

The most important change found when comparing CaHap spectrum with (Ca, Zn)Hap spectra, was the increase in the number of bands. The second derivative applied to CaHap spectra showed one $\nu_1(PO_4)$ band at 961 cm^{-1}, four bands for the $\nu_3(PO_4)$ mode and two for $\nu_4(PO_4)$ mode. In the OH^- librational region the absorbance and the second derivative spectra revealed only one band at 631 cm^{-1}. With Zn incorporation, however, the number of bands in the derivative spectra increases (see Table 4), six bands were detected for the $\nu_3(PO_4)$ mode, three for the $\nu_4(PO_4)$ mode and two for the libration mode of OH^- (640 and 632 cm^{-1}). Besides, as was also observed in the infrared spectra, the intensity of the OH^- libration band of CaHap (630 cm^{-1}) decreases with increasing zinc concentration.

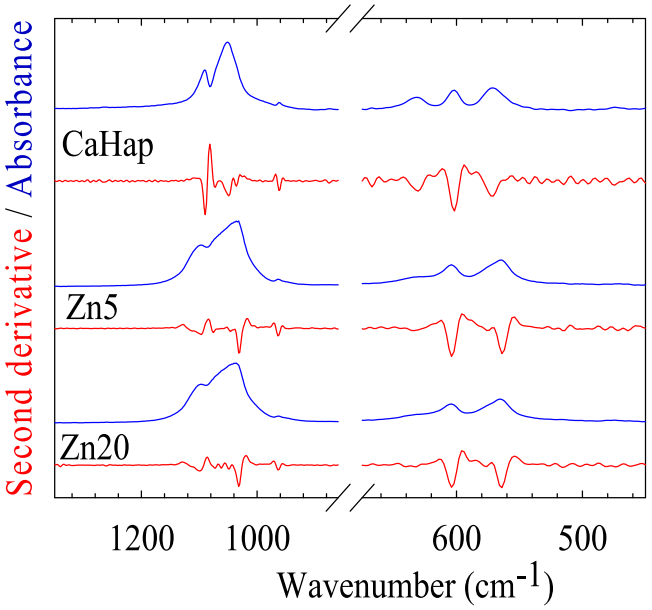

Fig. 3. Selected infrared spectra of CaHap and (Ca, Zn)Hap (blue) (Fig. 2), and their second derivative spectra (red). (For interpretation of the references to color in this figure legend, the reader is referred to the web version of this article).

To evaluate if the increment in the number of bands was due to a change in the crystal symmetry induced by Zn incorporation, XRPD patterns were obtained and a Rietveld analysis of data coming from selected samples was performed.

3.3. X ray powder diffraction

XRPD data as a function of 2θ, in the range $20 < 2\theta < 45°$, are shown in Fig. 4. As the Zn concentration augment an increase in the line widths and a reduction in their intensities was observed. Main changes were observed in the $30 < 2\theta < 35°$ range. These findings indicate increasing structural disorder or reduction in

Table 4
Wavenumbers for ν_3 and ν_4 PO_4^{3-} modes of CaHap and (Ca, Zn)Hap obtained from second derivative spectra.

Vibracional modes of PO_4^{3-}	CaHap	Zn5	Zn10	Zn15	Zn20
ν_{3a} (E_{1u})	1089	1112	1112	1114	N.D.[a]
		1100	1100	1102	1102
ν_{3a} (A_g)	1073	1074	1076	1076	1077
ν_{3a} (E_{2g})			1062	1065	1067
ν_{3c} (E_{1u})	1050	1043	1043	1046	1048
ν_{3b} (A_u)	1035	1031	1031	1031	1032
		999	999	999	999
ν_1 (A_g+E_{2g})	961	963	963	963	963
ν_{4a} (A_g)	602	604	604	604	604
ν_{4c} (E_{1u})	571	574	574	574	574
ν_{4a} (A_u)		563	563	563	563

[a] N.D: Not detected in the apatitic spectra of Zn20

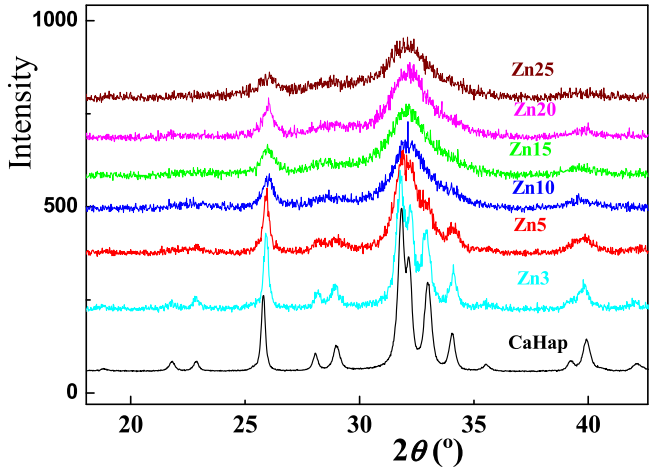

Fig. 4. X ray powder diffraction patterns a of CaHap and (Ca, Zn)Hap samples in the range $20 < 2\theta < 45°$.

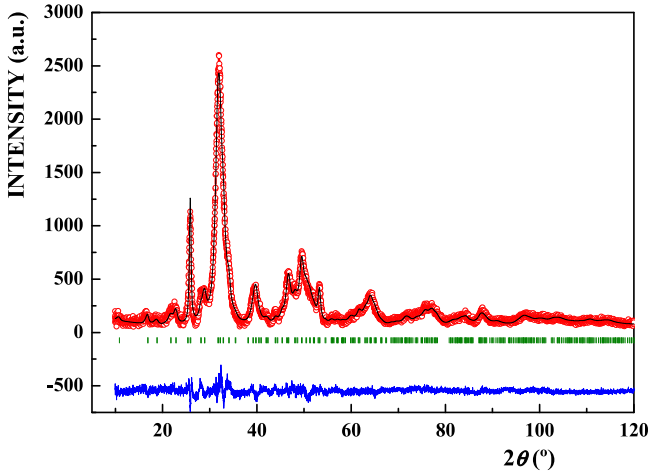

Fig. 6. Rietveld refinement analysis of sampleZn10.

Table 5
Crystal data and refinement details of CaHap and Zn10.

Crystal data		
Sample	CaHap	Zn10
System	Monoclinic	Hexagonal
Space Group	$P2_1/b$	$P6_3/m$
Cell constants		
a [Å]	9.3881(1)	9.4360(1)
b [Å]	18.774(1)	9.4360(1)
c [Å]	6.8910(1)	6.8793(1)
γ [°]	119.98(2)	120.0
V [Å^3]	1052.02(1)	530.46(1)
Rietveld analysis agreement factors		
R_{Bragg} [%]	3.7	3.7
R_p [%]	5.5	8.6
R_{wp} [%]	7.3	12.1
S	2.1	1.8

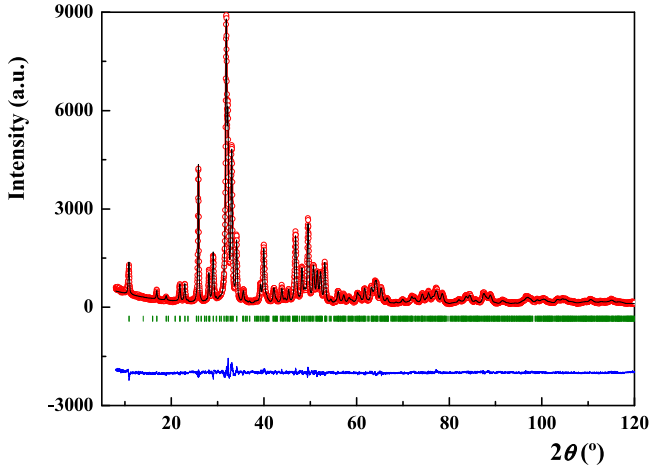

Fig. 5. Rietveld refinement analysis of sample CaHap.

crystallite sizes. To get a better understanding of how the Zn ions disturb the apatite structure, Rietveld analysis of the CaHap and Zn10 samples were carried out. The program Fullprof [41] was used to refine the structures of both samples, with form factors for cations Ca(II) and Zn(II) and anion O^{2-}, background was modeled with a fifth degree polynomial function. The March–Dollase model for preferred orientation was used, but it differed little from unity. A modified pseudo-Voight function was employed for lines profile. Diffractometer's zero was calibrated with and external standard. Parameters included in the refinement were: sample position, unit cell, scale, atoms fractional coordinates, overall and atomic isotropic thermal parameters and occupancy. The best structure refinement of CaHap was reached using as starting model the monoclinic hydroxyapatite structure, 93932-ICSD, obtained from the Inorganic Crystal Structure Database (ICSD) [44], while in the case of the Zn10 the best refinement was achieved starting from the hexagonal model of the CaHap with space group $P6_3/m$, obtained from Holly Springs hydroxyapatite [45] (26204-ICSD). Some relevant refinement parameters are listed in Table 5. The observed and calculated profiles of the CaHap and Zn10 samples are shown in Figs. 5 and 6 respectively. Atoms fractional coordinates, isotropic thermal parameters and occupation numbers are provided as supplementary material.

All the above results would indicate that the Zn(II) ion helps to stabilize the hexagonal CaHap structure and that the Zn(II) are incorporated in the apatite structure. When dealing with Zn10 sample, as noted previously by Ma and Ellis [28], it has been found that determination of site preference by Rietveld fitting to XRPD data is not unique.

It should be mentioned that Zn replacement by Ca1, Ca2 or both rendered similar agreement factors. However, a thorough analysis of the results has shown that replacement for Ca2 provides parameters consistent with the other characterization techniques results, see discussion. The values reported in Table 5 correspond to the selected fit, but the others are within 2%. The diminution of (Ca+Zn)/P ratio detected in Zn10 sample, shown in Table 1, could not be disclosed from the Rietveld refinement of present data.

3.4. Thermal behavior

In order to obtain additional information about the effect of Zinc substitution by Calcium, differential thermal analysis (DTA) and thermal gravimetric analysis (TGA) were performed to samples Zn3 to Zn20. In all the studied samples three regions of weight loss were identified in the TGA-curves: one between room temperature and about 200 °C (which can be safely assigned to adsorbed water), the second between about 200 and 500 °C and a third one between about 700 and 890 °C. It should be noted that in the range of 0–500 °C the mass loss increases with zinc concentration in the solid. This result was not observed at higher temperatures. Two endothermic peaks at about 50 and 750 °C were present in the DTA-curve of all analyzed samples.

TGA data are presented in Table 6. It can be noted from them

Table 6
Mass loss in the solid phases (expressed as mass fraction) obtained from TGA curves.

Sample	Mass fraction loss (%)				Total loss (%)
	(0–200 °C)	(200–500 °C)	(500–800 °C)	(800–1000 °C)	
Zn3	7.4	1.8	1.6	1.0	10.0
Zn5	10.6	3.1	1.7	0.9	13.2
Zn10	13.3	3.4	1.6	0.9	15.7
Zn20	14.3	3.7	1.9	0.5	16.7

that at 200 °C the mass loss is 7.4% for Zn3 and 14.3% for Zn20; these results reflect the increase of adsorbed water with zinc incorporation in the solid. Similar, but qualitative, results had been found previously by other authors [36,37]. To get insight into the different processes that take place during samples heating, infrared spectra of residues (from TGA–DTA) were taken for all Zn-substituted samples at selected temperatures (200, 500 and 700 °C). Representative spectra are shown in Fig. 8 (Zn5) and Fig. 9 (Zn20). These figures showed that the intensity of the broad bands located at about 3400 and 1634 cm^{-1} decreases drastically upon heating from 200 °C to 500 °C. This finding along with the simultaneous narrowing and shift to 1064 cm^{-1} of the phosphate vibration at 1035 cm^{-1} (ν_{3b} (A_u)), suggested elimination of hydrogen bonds linking phosphate anions and water molecules. The later have been removed by thermal heating.

Very weak bands, observed in the region 1456–1414 cm^{-1} for samples heated up to 500 °C, may be assigned to antisymmetric stretching (ν_3) of the CO_3^{2-} anion. An additional band (even weaker), at 876 cm^{-1}, from the bending mode of carbonate (ν_2) would confirm the presence of this anion in all samples. Due to the similar intensity observed for these bands in all samples below 500 °C, it can be safely assumed that the mass lost up to this temperature only corresponds to water.

According to previous studies, CaHap synthesized by precipitation method starts to decompose at around 800 °C and transforms to β-TCP ($Ca_3(PO_4)_2$) [4,9,13,16,22]. In present samples the most important change identified in phosphate vibrational modes occurred at 700 °C. Three new bands are observed at 1123, 981 and 928 cm^{-1}, corresponding to the $\nu_3(PO_4)$. Moreover, bands of phosphate bending modes at 603 and 564 cm^{-1} are shifted to 601 and 555 cm^{-1}. These changes evidence conversion of (Ca, Zn) Hap into β-T(Ca, Zn)P [$(Ca, Zn)_3(PO_4)_2$], which can be related to the feature observed at about 750 °C in the DTA curves. These results are in agreement with conclusions reported in the literature for similar systems [4,9,16,43].

Comparison of spectra of samples Zn5 and Zn20 heated at 700 °C (Figs. 8 and 9, respectively) evidenced disparities. Zn5 spectrum showed bands at 3572 and 630 cm^{-1} corresponding to OH^- vibrations, which are not observed in Zn20. Besides, ν(OH) band position in Zn5 (3572 cm^{-1}) was coincident with that of the as prepared CaHap (See Section 3.2.2). This implies that Zn cation

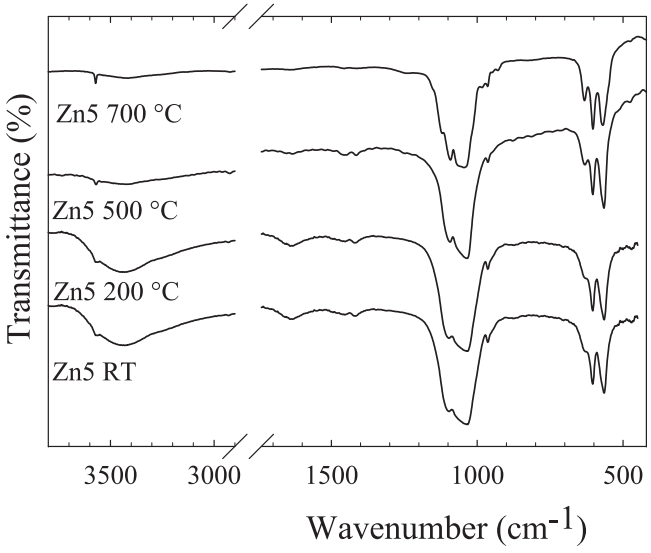

Fig. 8. Infrared spectra of thermally treated Zn5 sample. RT: Room temperature.

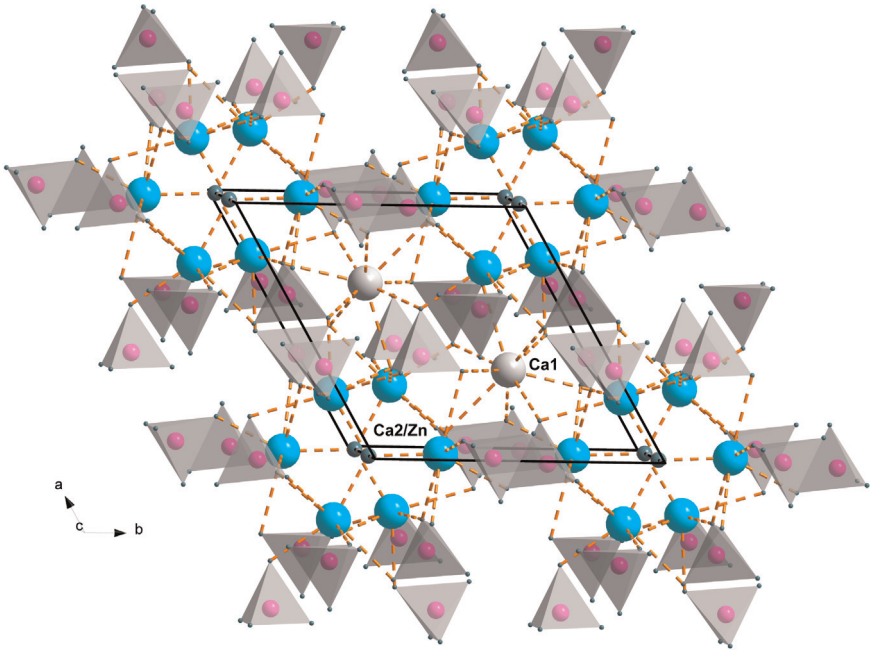

Fig. 7. Hydroxyapatite structure representation, view down c, showing Ca1 and Ca2 sites.

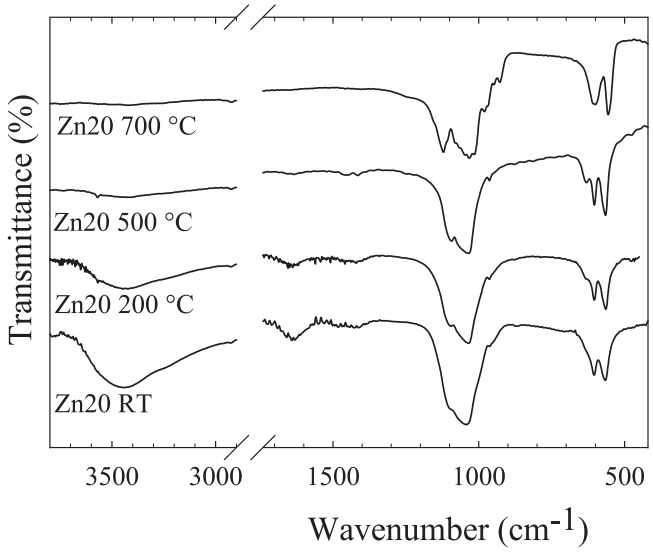

Fig. 9. Infrared spectra of thermally treated Zn20 sample. RT: Room temperature.

is not longer in the apatite phase, because in the CaHap doped with Zn the ν(OH) shifts to lower wavenumbers and the L(OH) shifts to higher wavenumbers, as pointed out in the mentioned section. Therefore, the Zn5 sample heated at 700 °C would be composed of a mixture of CaHap and β-T(Ca, Zn)P phases. At difference of Zn5, when Zn20 is heated up to 700 °C, its spectrum only shows bands at 1123, 1032, 980, 927, 601 and 555 cm^{-1}, corresponding to β-T(Ca, Zn)P. This result would support that (Ca, Zn)Hap sample was completed transformed into β-T(Ca, Zn)P in the Zn20 sample at 700 °C.

The IR spectra of both samples (Zn5 and Zn20), obtained after heating them at 700 °C, have not shown a band at 725 cm^{-1}, which would correspond to $P_2O_7^{4-}$, if this anion were present. This finding confirmed the previous assumption (based on the room temperature infrared spectra) that HPO_4^{2-} ion had not been incorporated in (Ca, Zn)Hap samples during the synthesis process.

4. Discussion

The chemical analysis results showed that not all the Zn(II) present in solution was incorporated into the synthesized (Ca, Zn) Hap structure for Zn3–Zn20 samples. In fact, although the concentration of zinc in the solid increased with Zn(II) content in solution, as shown in Table 1, the (Zn+Ca)/P relation decreased. The stoichiometric molar ratio value (Ca+Zn)/P is 1.67; values shown in Table 1 indicated that, for samples above Zn5, there is an increment of non stoichiometry in the solid as Zn(II) augment in the mother solution. The increase in Zn also produces broadening and intensity reduction of Raman bands. This is especially noticeable for the band at 960 cm^{-1} due to the symmetric stretching mode of phosphate. No signals of impurities could be detected from Raman spectra of CaHap and (Ca, Zn)Hap.

Comparison of CaHap infrared spectrum with spectra obtained from (Ca, Zn)Hap samples evidenced that bands position and intensity modifications were induced by Zn(II) incorporation. These changes are consistent with water content augment and OH^- drop as Zn increases. According to the band description presented above and from comparison of the spectra gathered in Fig. 2, it can be seen that the absorption of the OH^- groups shows interesting changes with Zn substitution. The L(OH) mode (632 cm^{-1}) is especially sensitive to substitutions in the apatite structure [13,50], its intensity correlates with the degree of crystallinity of CaHap [13,46,49,51]. With zinc incorporation the area of the L(OH) band decreases. In the same way, the OH^- stretching band, which appears in CaHap as a symmetrical and narrow peak at 3572 cm^{-1}, decreases its intensity and progressively shifts towards lower wavenumbers with the increase of zinc concentration in the solid (for 9.1% of zinc (Zn20) it is almost absent). This shift has been interpreted as due to hydrogen-bond formation [13,43,46]. According to Baddiel et al. [52], the oxygen atoms of the neighboring PO_4^{3-} groups are the only ones that can be comprised in such bonds. Oxygen atoms of both mentioned groups are close enough (3.05 Å) for O–H–OPO_3 bond to occur. On the contrarily, the distance between neighboring oxygen atoms belonging to OH^- groups is too large (3.44 Å) for a hydrogen bond between hydroxyl groups to be formed [13,52]. The band profile of PO_4^{3-} modes denotes the presence of a calcium apatite structure partially substituted for Zn. Bands located at 963 cm^{-1} (ν_1) and 473 cm^{-1} (ν_2), although infrared forbidden in tetrahedral symmetry [9,46,48], have infrared active components in the CaHap. These modes become active when the phosphate group is slightly distorted to specific symmetries lower than Td [47], giving rise to infrared bands of weak intensity which provide little information on its environment [13,43,48]. On the contrary, the ν_3 (1000–1100 cm^{-1}) and ν_4 (550–620 cm^{-1}) bands are infrared allowed in the theoretical free-ion spectrum and belong to the T_2 symmetry point group [48,49]. The splitting of these bands is due to the low site symmetry of the solid matrix and to intermolecular vibrational coupling [13,46–49].

As Nelson and Williamson [42] explained for carbonate ions, the incorporation of foreign ions in the apatite structure partially destroys the translational symmetry. In the present case, the substitution of calcium for zinc produces a distortion in the phosphate environment due to zinc cation smaller radius. Rietveld refinement analysis of the Zn10 XRPD data would indicate a distortion of the phosphate group. This distortion is consistent with the increment in the number of bands associated with vibrations of the PO_4^{3-}, observed from the infrared second derivative spectra; and with the intensity decrease and broadening increase of bands assigned to phosphate vibrations in Raman Spectra of the (Ca,Zn)Hap as prepared samples. The distorting effect of Zn(II) incorporation is stronger in present (Ca,Zn)Hap samples than in the carbonate apatite samples studied by Nelson and Williamson [42].

The intensity of the two broad bands shown in Fig. 2, at about 3400 and 1630 cm^{-1}, increases with zinc incorporation. The broadness observed in the ν(OH) bands (from water (3550–3200 cm^{-1}) and from OH^- group (3572 cm^{-1})) is caused by the H-bonding between molecules of adsorbed H_2O and between the water and the OH^- group of the apatite. All the above results suggest that the structural changes caused by partial substitution of Zn by Ca allows to accommodate more H_2O molecules, either adsorbed or bonded, into (Ca, Zn)Hap structure than in CaHap.

Zn3 to Zn20 spectra interpretation is consistent with XRPD data and analysis, which showed that Zn incorporation induces a modification of the space group of the CaHap, $P2_1/b$ to $P6_3/m$, and either a progressive loss of structural correlation or a decrease in grain size, which increases with Zn(II) augment in the solid. Inclusion of 25% molar (or higher concentrations) of Zn(II) in the reaction solution produces a poorly crystalline solid, its infrared spectrum allowed to detect a second phase ($ZnNH_4PO_4 \cdot H_2O$) in sample Zn25. This result would denote that the apatitic phase cannot incorporate into its structure more Zn(II) cations than those included in Zn20 sample, in agreement with findings of ref. 11 and 36.

It is known that the Ca-deficient apatite formed by the precipitation method incorporates H_2O, HPO_4^{2-}, CO_3^{2-} or other ions

for charge balance, resulting in changes in lattice parameters *a* and *c* [4,13,16,21,36]. According to these changes in present samples (Table 5), infrared spectra of Zn3 to Zn20 point to water and small quantities of CO_3^{2-} incorporation. The distortions of PO_4^{3-} group (described above) originate splitting of the typical spectrum coming from this group, which might mask the incorporation of HPO_4^{2-} in the Zn(II) doped samples. It should be remarked that in this work, the carbonate incorporation may be due to the absorption of atmospheric carbon dioxide by the alkaline solution during samples preparation. The intensity of carbonate bands did not increase with Zn incorporation. The low intensity of these bands might be due to the low level of CO_2 present throughout the reaction, and not necessarily implies that the (Ca, Zn)Hap can not accommodate more carbonate ions into its structure as Zn substitution grows.

The carbonate bands observed in the spectra of samples treated at 500 °C (see Figs. 8 and 9) indicate that carbonate ions have substituted some phosphate ions in the apatite lattice (B-type substitution) [4,11,17,51]. In biological apatites the predominant substitution appears to be CO_3^{2-} ions by PO_4^{3-} ions, but usually also occurs some OH^- ions replacement (A-type substitution) [48,51].

Infrared spectra of thermally treated samples and thermogravimetric studies results let to rule out the presence of HPO_4^{2-} in Zn(II) doped samples. Indeed the absence of the band at 725 cm^{-1} in thermally treated samples is an evidence of the absence of pyrophosphate ($P_2O_7^{4-}$), which might have been produced by decomposition of HPO_4^{2-} during the thermal treatment if the later anion had been present.

The above results allow to assume that positively charged vacancies were compensated by removing two OH^- ions for each Zn (II) (or Ca(II)) cation vacancy in the structure. Consequently, holes in the structure give rise to the incorporation of lattice H_2O in the solid. This interpretation is consistent with Rietveld analysis results, which have shown increase in lattice parameter *a* and decrase in parameter *c* with Zn(II) incorporation, Table 5. This finding, which agrees with others reported in the literature [36,37], is consistent with lattice H_2O substitution by OH in the apatite [11,13,48], so the influence of H_2O on (Ca, Zn)Hap crystallinity should also be considered.

The thermal study carried out on the (Ca, Zn)Hap solid samples prepared from aqueous media at 95 °C and pH 9 confirmed that the incorporation of Zn(II) ion helps to stabilize the hexagonal CaHap structure and that the Zn(II) were incorporated in the apatite structure. Replacement of Ca for Zn is contrary to Biggi et al. findings [46], these authors have assumed that Zn(II) was not incorporated to the structure, but adsorbed on the CaHap surface. They have also found that Zn affects CaHap crystallinity, as has been observed in present Zn(II) doped samples.

The CaHap crystal structure shows two crystallographycally inequivalent Ca(II) sites. As shown in Fig. 7 cations at site 1, Ca1, are coordinated by nine oxygens belonging to six PO_4^{3-} forming triangles and displaying a columnar arrangement. Cations at site 2, Ca2, are heptacoordinated by six oxygen atoms belonging to five PO_4^{3-} anions and one OH^- anion. The smallest distance between a cation and a coordinated oxygen is found at site 2, while the smallest Ca–Ca distances are observed between Ca(II) ions at site 1 [9,10,13,15,28]. Small ions (such as Cu(II) and Mg(II)) are incorporated preferentially in the CaHap structure at Ca1 [4,53,54]. In contrast, large cations (such as Sr(II), Ba(II) and Pb(II)) would first replace Ca(II) at Ca2 [4,11,21,29,48]. At difference of the expectation for small cations, the Zn(II) places at Ca2 sites of the stoichiometric CaHap. This assumption is based on Rietveld results and the noticeable modifications observed in the infrared signals coming from the OH^-groups which belong to the coordination sphere of calcium ions at Ca2. Ca(II) substitution at this site for a smaller ion, such as Zn(II), allows water to replace and/or bond to OH^- ions. Water inclusion induces changes in the vibrational spectra and loss of crystallinity. This interpretation is sustained by the observed crystallinity reduction and enhancement of changes in the vibrational spectra with Zn(II) content.

The total mass loss (expressed as the mass fraction) found in the thermogravimetric studies of samples heated continuously from 30 °C to 1000 °C in a nitrogen atmosphere (see Table 6), indicated that water molecules present in the samples are either adsorbed or incorporated into CaHap structure. Most of the water molecules are lost in the range 0–200 °C, making evident that Zn(II) incorporation in the solid favors water adsorption. In turn, lattice water is lost in the 200–500 °C temperature range. Variations of lattice water content can only be appreciated when going from Zn3 to Zn5. The results also show that the amount of lost water increases with Zn(II) content in the solid. This may be due to the concomitant incorporation of Zn(II) and CO_3^{2-}, so a model with cationic and anionic vacancies (OH^-), the later being partially substituted by water, has been considered. This model does not agree with Miyaji et al. findings [36]. These authors have observed an increased amount of lattice H_2O (which replace OH^-) in the apatite structure as zinc substitution grows, but they have not found carbonate ions incorporated in the structure during the synthesis. The dissimilarity found is probably due to differences in the synthesis conditions (inert atmosphere and shorter stirring time, 5 h).

Since the presence of HPO_4^{2-} group could be discarded, only lattice H_2O and carbonate ion decomposition might be responsible for the weight loss in the 500–750 °C temperature range. Therefore, the thermal process at 700 °C can be represented by the following reactions, for samples Zn3 to Zn15:

$$(Ca,\ Zn)_{10}(PO_4)_{6-x}CO_{3x}(OH)_2 \rightarrow \beta\text{-}(Ca,\ Zn)_3(PO_4)_2 + Ca_{10}(PO_4)_6(OH)_2 + H_2O + CO_2$$

and for sample Zn20:

$$(Ca,\ Zn)_{10}(PO_4)_{6-x}CO_{3x}(OH)_2 \rightarrow \beta\text{-}(Ca,\ Zn)_3(PO_4)_2 + H_2O + CO_2$$

The infrared analysis of the powders obtained after thermal treatment showed the formation of the ß-TCP phase, whose presence becomes increasingly evident as the zinc concentration in the solution was augmented. The substitution of a few percent of calcium for zinc leads to the partial thermal conversion of (Ca, Zn) Hap into ß-T(Ca, Zn)P. The formation of ß-T(Ca, Zn)P is a sensitive indicator of a composition with Ca/P ratio lower than that one corresponding to stoichiometric CaHap [3,10,13,43]. The most likely explanation for the existence of ß-TCP phase in the heated (Ca, Zn)Hap powders is that the presence of zinc in the reaction solution leads to the formation of a calcium deficient apatite that has a Ca/P ratio less than 1.67 and contains CO_3^{2-} groups and water molecules. Calcium-deficient hydroxyapatites are thermally less stable than stoichiometric CaHaps. For example, the formation of ß-TCP at about 725 °C occurs only in the Zn20. In the rest of the samples studied this transformations occurs at 760 °C. Furthermore, when heated to above 750 °C, calcium deficient CaHap decomposes into β-$Ca_3(PO_4)_2$ plus some residual apatite but if the Ca/P ratio is lower than 1.5 (Zn20) there would not be residual apatite, as detected after this treatment.

An ideal material for prostheses and implants should degrade inside defects simultaneously with new bone formation. In this way full restoration of the defect with biological materials will be achieved. It is known that CaHap is more stable than α- and ß-TCP under physiological conditions, as it has a lower solubility and lower resorption kinetics [3]. Implants of calcinated CaHap of high crystallinity would remain in defects, even years after implantation, in virtually unchanged form. Therefore, ß-TCP or BCP (biphasic calcium phosphate) ceramics are favored as implant materials at present [3].

The results presented above demonstrated that a Ca-deficient

apatite doped with zinc could be prepared up to Zn 9.1 wt%. At higher concentrations, Zn(II) doping shows inhibitory effect on apatite formation. Besides, thermal and crystallographic studies have shown that (Ca, Zn)Hap with zinc content below to 6.5 wt% have a thermal stability and structure comparable to those ones of animal bones [48,55] Moreover, the inclusion of vacancies and other substituents like CO_3^{2-} and water in the apatite crystal lattice makes its structure closer to natural bone crystal [4,10,48,55] Since (Ca, Zn)Hap is less stable than CaHap, it seems reasonable to assume that (Ca, Zn)Hap would be more soluble than CaHap under physiological conditions. This property may be useful in bone repair applications requiring calcium phosphate with biodegradation properties lower than those of ß-TCP but higher than those of CaHap.

5. Conclusions

The precipitation method used in this work allows the incorporation of Zn(II) in the CaHap structure up to 9.1% (sample Zn20), as determined by absorption spectroscopy. The analysis of infrared, Raman and XRPD results clearly shows that low Zn(II) inclusion favors the formation of an hexagonal CaHap, whose crystallinity decreases and water content increases as Zn(II) concentration in the solid augment. Concentrations higher than 9.1% (Zn25 sample) produce a phase mixture with a higher amorphous character. Rietveld analysis results, supported for vibrational spectra and thermal data, allow to assume that in present samples Zn(II) exhibits preference to occupy the Ca2 site of the apatite structure. The information obtained in this work suggests that (Ca, Zn)Hap doped with zinc below 6.5 wt% may be a promising biomaterial useful in bone repair applications requiring calcium phosphate with biodegradation properties higher than those ones of the stoichiometric CaHap.

Acknowledgements

The authors acknowledge National Scientific and Technological Research Council of Argentina (CONICET) projects: PIP0985 and PIP0327; Universidad Nacional de La Plata (UNLP, Argentina)) Projects 11X/577, 11X565, 11X672 and 11X/709 and Departamento de Ciencias Básicas de la Universidad Nacional de Luján (UnLu, Argentina) for financial support projects B112 and B152 for financial support. G.A.E., J.A.G., G.P. and R.V. are members of CONICET.

Appendix A. Supplementary information

Supplementary data associated with this article can be found in the online version at http://dx.doi.org/10.1016/j.jpcs.2015.01.017.

References

[1] R.Z. LeGeros, G. Quirolgico, J.P. LeGeros, J. Dent. Res. 60B (1981) 452–458.
[2] J. Christoffersen, M.R. Christoffersen, N. Kolthoff, O. Barenholdt, Bone 20 (1997) 47–54.
[3] S.V. Dorozhkin, M. Epple, Angew. Chem. Int. Ed. 41 (2002) 3130–3146.
[4] R.Z. LeGeros, Lippincvott Williams & Wilkins, Clin. Orthop. Relat. Res. (2002) 81–98.
[5] A. Yasukawa, K. Kamiuchi, T. Yokoyama, T. Ishikawa, J Solid State Chem. 163 (2002) 27–32.
[6] A.S. Karpov, J. Nuss, M. Jansen, P.E. Kazin, Y.D. Tretyakov, Solid State Sci. 5 (2003) 1277–1283.
[7] G.M. Blake, I. Fogelman, J. Bone Miner. Res. 20 (2005) 1901–1904.
[8] C. Ergun, T.J. Webster, R. Bizios, R.H. Doremus, J. Biomed. Mater. Res. 59 (2002) 305–311.
[9] J.C. Elliot., Elsevier Science B. V. (ed) Amsterdam, Structure and Chemistry of the Apatites and Other Calcium Orthophosphates, Amsterdam, The Netherlands (1994) 20–95.
[10] J.C. Elliott, The Mineralogical Society of America, 1015 Eighteenth Street, NY, Suite 601, Washington, DC (2002) 427–453.
[11] R.Z. LeGeros, L. Singer, R.H. Ophaug, G. Quirolgico, A. Thein, J.P. LeGeros, in: J. Menczel, G.C. Robin, M. Makin, R. Steinbeg (Eds.), Osteoporosis, Wiley, New York, 1982, pp. 327–341.
[12] S. Kannan, J.M.F. Ferreira, Chem. Mater. 18 (2006) 198–203.
[13] J.R. Guerra-López, R. Pomés, C.O. Della Védova, R. Viña, G. Punte, J. Raman Spectrosc. 32 (2001) 256–261.
[14] S.Y. Azimov, A.A. Ismatov, N.F. Fedorov, Inorg. Mater. 17 (1981) 1384–1387.
[15] J.L. Lacout, A. Nounah, M. Ferhat, Ann. Chim. Sci. Mater. 23 (1998) 57–60.
[16] S. Neuman, M. Nele, V.M.M. Salim, Thermochim. Acta 451 (2006) 16–21.
[17] C. Rey, in: A. Zahid (Ed.), Calcium phosphates in biological and industrial systems, Kluwer Academic Publishers, Boston, 1998, pp. 217–251.
[18] E. Fujii, M. Ohkubo, K. Tsuru, S. Hayakawa, A. Osaka, K. Kawabata, C. Bonhomme, F. Babonneau, Acta Biomater. 2 (2006) 69–74.
[19] A. Corami, S. Mignardi, V. Ferrini, J. Colloid Interface Sci. 317 (2008) 402–408.
[20] A. Bahdod, S. El Asri, A. Saiabi, T. Coradin, A. Laghzizil, Water Res. 43 (2009) 313–318.
[21] J.C. Elliot, Elsevier Science B. V.. (ed) Amsterdam, Structure and Chemistry of the Apatites and Other Calcium Orthophosphates, Amsterdam, The Netherlands (1994) 63–110.
[22] Z.Y. Lia, W.M. Lama, C. Yangb, B. Xub, G.X. Nia, S.A. Abbaha, K.M.C. Cheunga, K. D.K. Luka, W.W. Lua, Biomaterials 28 (2007) 1452–1460.
[23] D. Laurencin, N. Almora-Barrios, N.H. De Leeuw, C. Gervais, C. Bonhomme, F. Mauri, W. Chrzanowski, J.C. Knowles, R.J. Newport, A. Wong, Z. Gan, M. E. Smith, Biomaterials 32 (2011) 1826–1837.
[24] M. Yamagichi, R. Yamaguchi., Pharmacology 35 (1986) 773–777.
[25] M. Hashizume, M. Yamaguchi, Mol. Cell. Biochem. 122 (1993) 59–64.
[26] B.S. Moonga, D.W. Dempster, J. Bone Miner. Res. 10 (1995) 453–457.
[27] A. Ito, K. Ojima, H. Naito, N. Ichinose, T. Tateishi, J. Biomed. Mater. Res. 50 (2000) 178–183.
[28] M. Xiaoyan, Donald E. Ellis, Biomaterials 29 (2008) 257–265.
[29] D. Bazin, X. Carpentier, I. Brocheriou, P. Dorfmuller, S. Aubert, C. Chappard, D. Thiaudiere, S. Reguer, G. Waychunas, P. Jungers, M. Daudon, Biochimie 91 (2009) 1294–1300.
[30] A. Ito, H. Kawamura, S. Miyakawa, P. Layrolle, N. Kanzaki, G.L. Treboux, J. Biomed. Mater. Res. 60 (2002) 224–231.
[31] A. Ito, M. Otsuka, H. Kawamura, M. Ikeuchi, H. Ohgushi, Y. Sogo, N. Ichinose, Curr. Appl. Phys. 5 (2005) 402–406.
[32] Y. Sogo, I. Atsuo, K. Michimasa, T. Sakurai, K. Onuma, N. Ichinose, M. Otsuka, R. Z. LeGeros, Mater. Sci. Eng. C 24 (2004) 709–715.
[33] H.K.A. Chou, R.Z. LeGeros, Z. Chen, L. Yihong, Implant Dent. 16 (2007) 89–100.
[34] S. Jenkings, M. Addy, J. Clin. Periodontol. 16 (1989) 385–387.
[35] R.Z. LeGeros, C.B. Bleiwas, M. Retino, R. Rohanizadeh, J.P. LeGeros, Am. J. Dent. 12 (1999) 65–70.
[36] F. Miyaji, Y. Kono, Y. Suyama, Mater. Res. Bull. 40 (2005) 209–2020.
[37] R. Fuzeng, X. Renlong, G. Xiang, L. Yang, Acta Biomater. 5 (2009) 3141–3149.
[38] E. Hayek, H. Newesely, Inorg. Syn. 7 (1963) 63–66.
[39] G.J. Bates, Res. Natl. Bur. Std. (US). 66a, 1962, 179–181.
[40] J. Portal., BSc. Thesis, Havana University. 1994.
[41] J. Rodríguez-Carvajal, Physica B 192 (1993) 55–69.
[42] D.G.A. Nelson, B.E. Williamson, Aust. J. Chem. 35 (1982) 715–720.
[43] J. Guerra-López, A. Gómez, R. Pomés, G. Punte, C.O. Della Védova, J. Solid State Chem. 151 (2000) 163–169.
[44] A. Belsky, M. Hellenbrandt, V.L. Karen, P. Luksch, Acta Cryst. B58 (2002) 364–369.
[45] K. Sudarsanan, R.A. Young, Acta Crystallogr. B 25 (1969) 1534–1543.
[46] A. Bigi, E. Foresti, M. Gandolfi, M. Gazzano, N. Roveri, J. Inorg. Biochem. 58 (1995) 49–58.
[47] B.O. Fowler, Inorg. Chem. 13 (1974) 194–207.
[48] J.C. Elliot, Elsevier Science B. V. (ed) Amsterdam, Structure and Chemistry of the Apatites and Other Calcium Orthophosphates, Amsterdam, The Netherlands (1994) 169–225.
[49] Y. Leung, M.A. Walters, R.Z. LeGeros, Spectrochim. Acta A 46 (1990) 1453–1459.
[50] C. Castro Ribeiro, I. Gibsond, M.A. Barbosa, Biomaterials 27 (2006) 1749–1761.
[51] J.C. Elliot, Elsevier Science B. V. (ed) Amsterdam, Structure and Chemistry of the Apatites and Other Calcium Orthophosphates, Amsterdam, The Netherlands (1994) 191–281.
[52] C.B. Baddiel, E.E. Berry, Spectrochim. Acta 22 (1966) 1407–1416.
[53] A. Tamperi, G. Celotti, E. Landi, M. Sandri, Key Eng. Mater. 264–268 (2004) 2051–2054.
[54] S. Spiro, G. Pezzotti, G. Celotti, E. Landi, A. Tamperi, J. Mater. Res. 20 (2005) 1009–1016.
[55] J.C. Elliot., Elsevier Science B. V. (ed) Amsterdam, Structure and Chemistry of the Apatites and Other Calcium Orthophosphates, Amsterdam, The Netherlands (1994) 259–304.